Evolution and System Dependent Properties of Zonal Flows and GAMs in Tokamaks and Planet Atmospheres

K. Hallatschek[1] and A. Kammel[1]

[1]Max-Planck-Institute for Plasma Physics, Garching, Germany

Corresponding Author: Klaus.Hallatschek@ipp.mpg.de

Abstract:
We have studied the evolution of the zonal flows (ZF) in first principles turbulence simulations, while artificially controlling the starting conditions or time dependence of the flows to find the rules governing the flow evolution, the preferred, stable and unstable states. A functional describing the parallel and perpendicular Reynolds stresses has been determined, which inserted into a 1D momentum balance equation is able to reproduce the evolution of the self-consistent radial ZF pattern from noise to the stationary state. Thereby a qualitative difference was discovered between toroidal ion temperature gradient (ITG) turbulence and sheared cylinder resistive drift wave (DW) turbulence induced flows. While in the ITG case, the wavelength of the flow pattern is fixed independent of the initialization, the DW turbulence maintains the period of any initialized pattern while enforcing a square wave shearing rate profile. For the GAMs the deterministic part of the turbulence dramatically changes the dispersion relation, resulting in orders of magnitude higher radial drift speeds and determines the preferred GAM wavenumber. This can lead to bursting GAM and turbulence activity, which depends on the sign of the grad-B drift with respect to the closest X-point. A comparative study of rotating planetary (Jovian) turbulence using the novel NAN (Navier Stokes, anelastic turbulence) code incorporating the associated density contrasts, shows that here ZFs are being generated similarly by a Reynolds stress based self amplification, control turbulence (bursting and profile modulation is observed).

1 Tokamak core turbulence

Although the global flows largely determine the anomalous transport in magnetically confined plasmas [1, 2], apart from extremely reduced analytic models and numerically calculated (linear) secondary/tertiary instabilities not much is known about the time evolution of the zonal flows (ZF) of the core and geodesic acoustic modes (GAM, essentially oscillating ZF) of the edge region. This is despite the flows resulting from a turbulent self amplification process, which renders their behavior deterministic when the system is large enough to average over many turbulent vortices (most current experiments).

The overarching outcome of our studies is that the time evolution of the ZFs becomes completely deterministic for sufficiently large computational domains. This is demon-

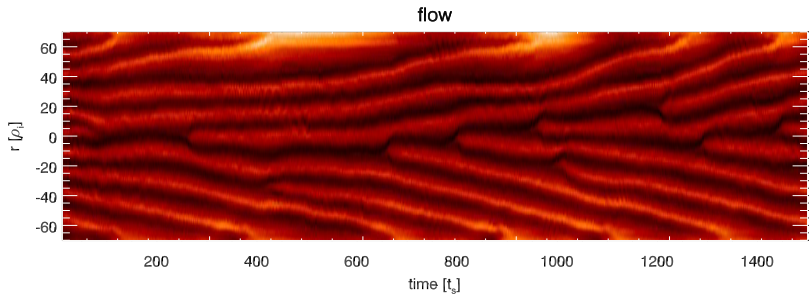

FIG. 1: Result of core ITG turbulence run; flux surface averaged ZF velocity (color coded) as a function of minor radius and time. Even though the flows continue to drift out of the computational domain (a boundary effect), a specific radial wave number is maintained by the turbulence by generating new flow minima and maxima. The wave number of the flows is robust.

strated in fig. 1, which is shows the typical behavior of ZFs under tokamak core conditions ($q \sim 1-2$, $L_n, L_T \sim R$) driven by ITG turbulence. The flows are totally constant in magnitude and wave form, apart from a steady drift out through the boundaries. Due to the outward drift, the wavelength of the flows increases, which is evidently not tolerated by the system – it generates more ZF maxima (in electron diamagnetic direction) to fill the voids. The loss of ZF peaks out of the computational domain is of course a property due to the particular (necessarily to some degree artificial) boundary conditions used in the simulation and can be avoided by prescribing the ZF velocity at the boundary, which renders the flow pattern completely stationary (not shown).

To understand this time evolution, We have studied the evolution of the global flows in first principles two-fluid and gyrokinetic turbulence simulations, while artificially controlling the starting conditions or time dependence of the flows to find the rules governing the flow evolution, the preferred, stable and unstable states, and the influence of inhomogeneities, i.e., the effects of the boundary conditions and of radially varying plasma parameters and other non-Boussinesq effects [3].

That way and taking into account restrictions by physical symmetries, for the global flows a robust functional describing the parallel and perpendicular Reynolds stresses has been derived,

$$R_{\perp,\parallel} = Q(au - b\partial_r^2 u - c\partial_r^4 u - du^3 - e\partial_r \ln Q), \tag{1}$$

based on the radial turbulent heat flux, Q, as measure of the turbulence level, and the flow shear $u = \partial_r v_\theta$, with empirically determined coefficients a, b, c, d, e, $(a, c, d, e > 0)$. This ansatz describes robustly the Reynolds stress even for flow induced turbulence level swings of over an order of magnitude (see fig. 2), and in a 1D momentum balance equation is able to reproduce the evolution of the self-consistent radial ZF pattern from noise to the stationary state. An indispensable feature are thereby the two wavenumber scales prescribed by the ratio of the coefficients a, b, c $(b > 0)$, which are the minimum necessary to represent a local *maximum* in the ZF growth rate. Without only two coefficients (one scale length) only the maximum wavelength is stable.

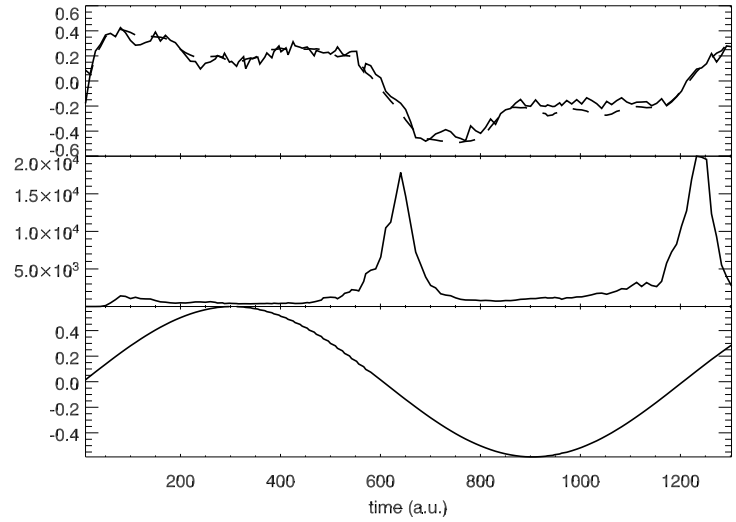

FIG. 2: Local turbulence stress response to sinusoidal shear flow pattern. Upper plot: perpendicular turbulent Reynolds stress rescaled to local heat flux $\pi_{\theta r}/Q$ (solid), phenomenological ansatz $\pi_{\theta r}/Q \approx \alpha\partial_r v_\theta(1-\beta\partial_r v_\theta^2) - \gamma\partial_r \ln Q$ (dashed); middle plot: local instantaneous turbulent heat flux Q; lower plot: local imposed shearing rate $\partial_r v_\theta$. The nonlinear term and the heat flux dependent term are necessary to account for the saturation and the asymmetries of the Reynolds stress response. Note the quality of the functional representation despite the large variation in heat flux.

2 Sheared slab drift wave turbulence

For sheared cylinder resistive drift wave (DW) turbulence of suitable parameters we also obtain deterministic turbulence induced flows. As for core ITG turbulence the final state consists of periodic alternating regions of positive or negative shearing rate at a fixed saturation level. However, the actually established pattern depends on the history of the system. This becomes apparent when comparing in fig. 3 the end state for a DW simulation started from noise (a) and (b) the one for a simulation started from a prescribed initial sinusoidal ZF pattern with an arbitrary wavelength (but similar shearing rate as in the other case). The turbulence does not attempt to alter the period of the initial pattern and only "rectifies" the shearing rate of the sine, transforming the flow into a triangular wave form. Both patterns (a) and (b) have been followed for a very long time and are indefinitely stable. In a way, the DW-ZF system can be regarded as a digital storage medium with two admissible flow shear states, while the ITG-ZF system has no memory. Evidently in the DW system the ratio of the parameters a, b, c only prescribes a *minimum* wavelength and may be replaced to good approximation by one with $b < 0$, $d = 0$. !!!!!

Different from the expectations, we find that ZF do not occur for all possible DW parameters, which is due to the variation of the interaction of DWs with their respective resonant surfaces, which also strongly influences the transport scaling.

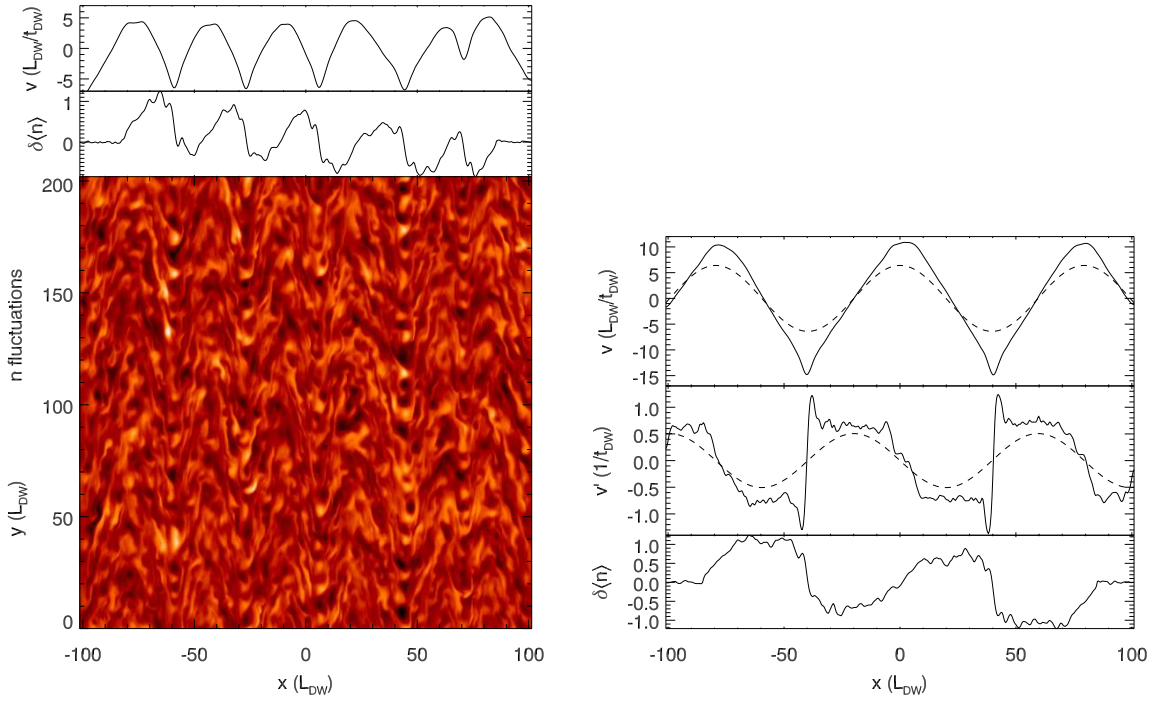

FIG. 3: Result of slab drift wave turbulence simulation. Left: end state of flux surface averaged ZF velocity as a function of radial coordinate (x) (top), concomitant flux surface averaged density corrugation (middle) and instantaneous turbulent density perturbations in a cross section of the 3D computational domain (bottom); right: initial (dashed) and final (solid) ZF velocity (top), shearing rate (middle) and density corrugations (bottom) for identical parameters as on the left, except for a pre-initialized zonal flow with long wavelength. The end states are completely stationary in both cases. The wavelength is evidently not prescribed by the turbulence, but the shearing rate is.

3 Tokamak edge turbulence/GAMs

For the GAMs relevant for the tokamak edge ($q \sim 3-5$) the deterministic part of the turbulence changes the dispersion relation, resulting in orders of magnitude higher radial drift speeds, since the linear curvature drift effects are augmented by turbulent transport. Second it determines the preferred GAM wavenumber, which for non-symmetric plasma geometries can be signed corresponding to inward or outward phase speed. The *nonlinear* dispersion relation can be impressively seen in the GAM wave pattern due to the resulting reflection at a *nonlinear* cutoff layer [4, 5, 6, 7, 8]. A preferred sign of the wavenumber can result in bursting GAM and turbulence activity, which depends on the sign of the ∇B drift with respect to the closest X-point.

4 Planetary turbulence

Since planetary and magnetized plasma turbulence are similar beyond mere two-dimensional nature (e.g., planetary Rossby waves are a close analogue of plasma drift waves) a comparative study of rotating planetary (Jovian) turbulence using the novel NAN (Navier Stokes, anelastic turbulence) code has been initiated to study (deep) Jovian turbulence, including the strong non-Boussinesq effects due to the density contrast between the top and bottom of the atmosphere.

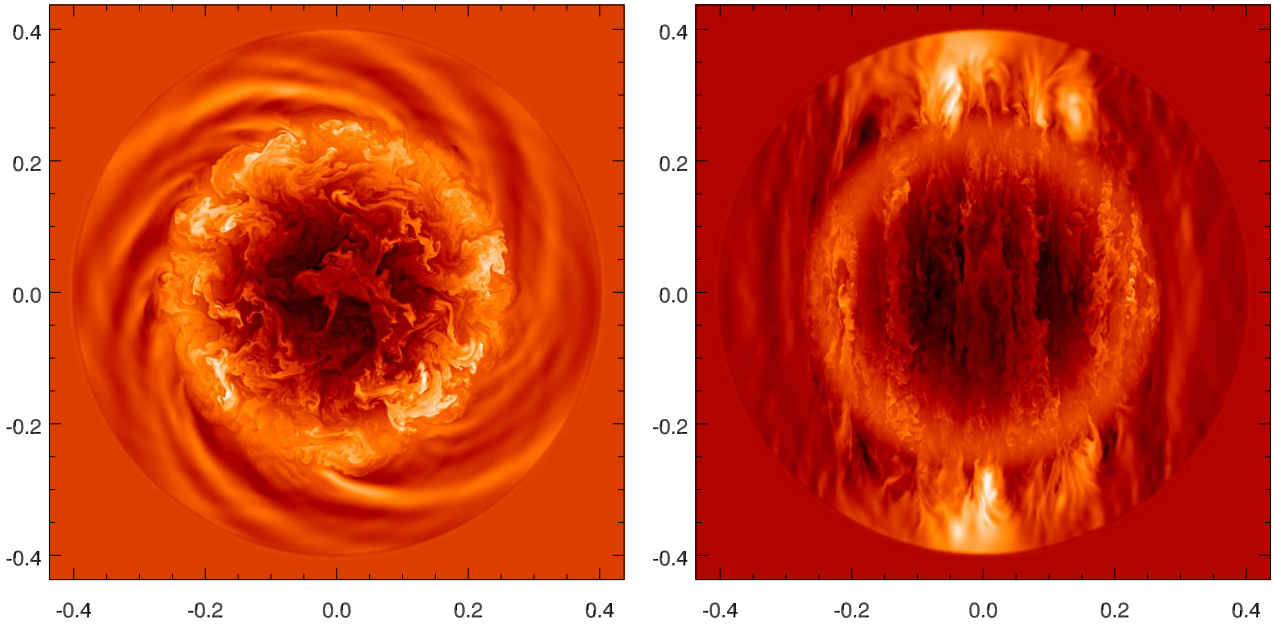

FIG. 4: Entropy fluctuations at the beginning of a planetary simulation with 1024^3 *grid points and a density ratio of 10 between the core and the surface of the planet. The system is unstable inside radius 0.27 due to initialization with a negative radial entropy gradient. Further outside the system is stable, resulting in the radiation of relatively smooth gravity waves. Left: equatorial cross section viewed from the top; the turbulence appears isotropic. Right: cross sectional plane parallel to the planet's rotation axis; structures above a threshold size are aligned with the axis.*

The exact hydrodynamic equations can be written favorably in terms of specific entropy s and enthalpy h as

$$\partial_t \boldsymbol{v} + \boldsymbol{v} \cdot \nabla \boldsymbol{v} + 2\boldsymbol{\Omega} \times \boldsymbol{v} = -\nabla(h + \phi) + T\nabla s \tag{2}$$

$$\partial_t s + \boldsymbol{v} \cdot \nabla s = 0 \tag{3}$$

$$\partial_t h + \boldsymbol{v} \cdot \nabla h = -\kappa_s(h)^{-1} \nabla \cdot v \tag{4}$$

where $\boldsymbol{v}, \boldsymbol{\Omega}$ are the velocity field and the angular velocity vector of the planet, and $\phi, T(h,s), \kappa_s(h,s)$ are the gravitational potential (assumed constant in time), temperature and isentropic compressibility (for an ideal gas with f degrees of freedom $\kappa_s = f/(2h)$).

The isentropic sound waves are described by the time derivative in eq. (4) [together with the momentum equation (2)]. To avoid excessively small time-steps due to the

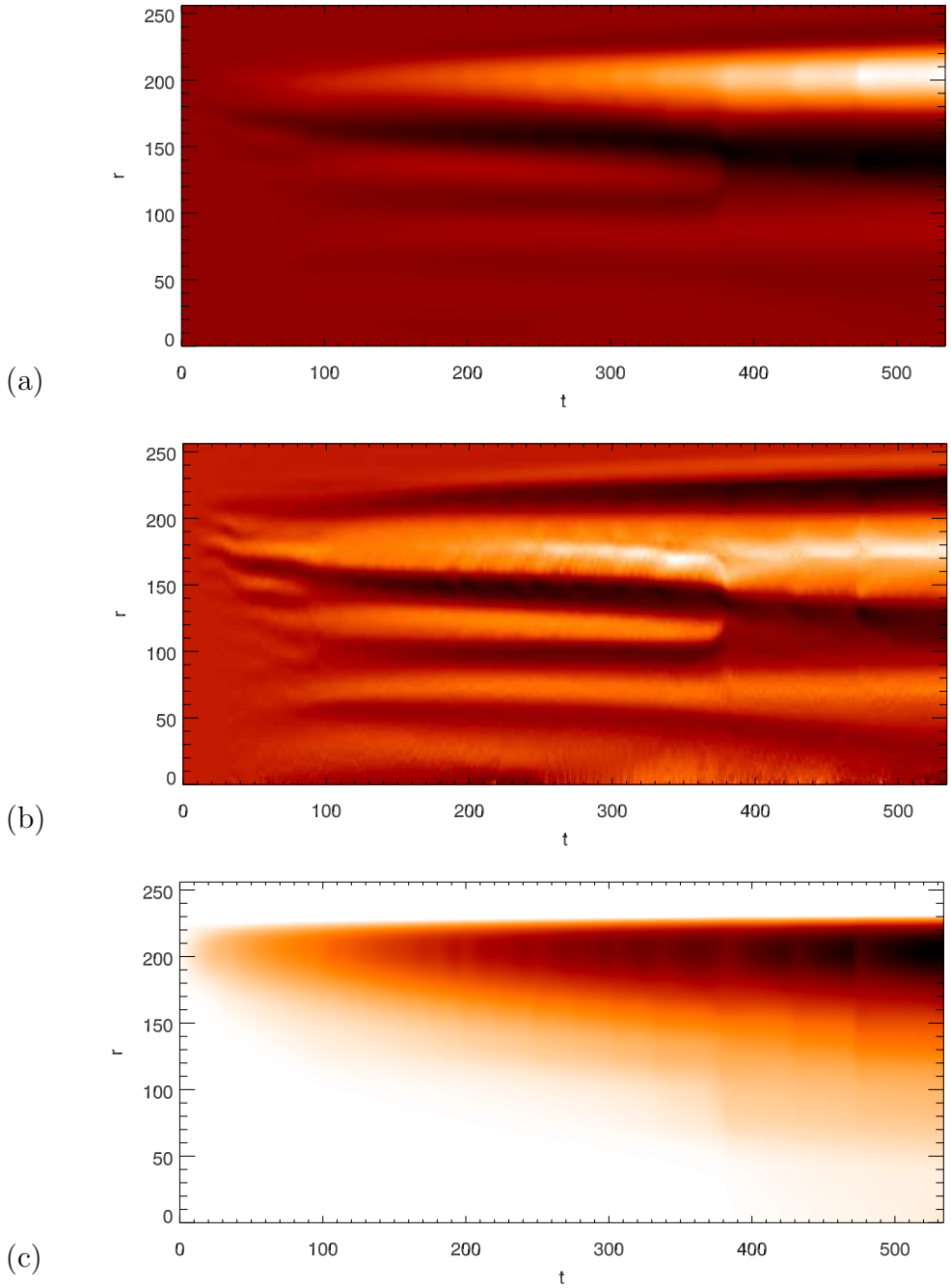

FIG. 5: Time dependent azimuthal averages of poloidal momentum (a) and vorticity (b) as a function of distance of the planetary axis, and spherical averages of the entropy (c) as a function of radius for a planetary turbulence simulation with a density contrast of 10, $\Omega = 1000$ *and a total cooling rate of* 0.5 *and a planetary radius* 0.4. *The radius unit in the figures is 0.002.*

Courant condition, the code eliminates the sound waves either by treating h implicitly, or at even lower computational cost by using the *anelastic limit* by neglecting the partial

time derivative in eq. (4) and nevertheless using it to solve for h. This is equivalent to consistently determine the field h, such that the *anelastic* condition [9] for the velocity

$$\nabla \cdot (n\boldsymbol{v}) = 0 \tag{5}$$

is maintained.

The code is setup with a Cartesian, so that fast methods can be used to calculate h at every time step, allowing efficient parallelization and the use of unprecedented resolution. Fig. 4 shows entropy fluctuations in two different cross sections at the same instant of time for a simulation started from an initially unstable entropy profile in the center. They exhibit clearly the Taylor-Proudman alignment of turbulent structures by the strong Coriolis force due to the rotation. It is also evident that the alignment ceases at sufficiently small scales where the planetary frequency becomes negligible compared to the eddy spin rate (which is the reason why a 3D simulation is necessary).

Realistic turbulence simulations are started from a neutral (i.e. constant) entropy profile, and driving it by a constant cooling rate localized at the surface of the planet. For sufficiently high Ω and sufficiently low turbulence drive, ZFs are generated as shown in fig. 5a,b. Similar to ZFs in tokamak core turbulence or slab drift waves, the planetary ZFs grow first at relatively short scales. Due to the specific geometry of the planet, a positive (eastward) flow is always generated at the equator (equatorial super-rotation). With time the flows slowly shift around, showing clear evidence of an effective repulsive force. Different from both plasma scenarios, the ZFs exhibit neither a preferred finite scale length nor a long term memory effect, but instead converge to just one equatorial jet and a counter rotation of the rest of the planet. (Clearly the annihilation of the multiple flows in favor of just one equatorial flow is incompatible with the observations of the large giant planets – it may however rather represent the solar tachocline. It is likely that at different parameters one might recover a behavior similar to the tokamak core, where a finite ZF wavelength results.) In addition bursts of turbulence activity are occur as evidenced by steps in the entropy profile (fig. 5c) and sudden increases in the ZFs (which are driven by the turbulence). The bursts are essentially caused by a thresholding behavior in the gradient drive of the turbulence, which varies in time as here the cooling rate is kept constant.

The basic evolution of the planetary flows lends itself to the same phenomenological treatment as the plasma flows, based on a Reynolds stress functional of the flow pattern and the turbulence intensity – with altered parameters.

A representation of the flow evolution by a model of *vorticity* transport [10] based on a functional of certain profiles of the system is unlikely (or at least impractical), since momentum conservation restricts the allowed vorticity flux in so far as the have to be a certain *radial derivative*. On the other hand, an arbitrary momentum flux automatically maintains vorticity conservation. This essentially means that the momentum transport is the basic quantity that should be analytically or empirically described in terms of the macroscopic system state.

5 Conclusions

We have found large similarities and subtle differences in the behavior of ZFs for various plasma systems and for planetary turbulence. In all systems the flows can be described by a deterministic Reynolds stress response functional based on radial profiles of the system indicating direct (non-local) interaction of small scale turbulence and flows and speaking against flow generation by inverse cascades. The flow level and scales are thereby controlled by the turbulence, and not by a linear dissipation mechanism acting on the flows.

References

[1] P.H. Diamond, S.-I. Itoh, et al., Plasma Phys. Control. Fusion **47**, R35 (2005)
[2] K. Hallatschek, Plasma Phys. Control. Fusion **49**, B137–B148 (2007)
[3] K. Hallatschek, et al. Phys. Plasmas **7**, 2554 (2000)
[4] R. Hager, K. Hallatschek, Phys. Rev. Lett. **108**, 035004 (2012).
[5] R. Hager, K. Hallatschek, Phys. Plasmas **16**, (2009) 072503
[6] R. Hager, K. Hallatschek, Phys. Plasmas **17**, (2010) 032112
[7] K. Hallatschek, et al., *Phys. Rev. Lett.* **86**, 1223 (2001)
[8] K. Hallatschek, G. R. McKee, Phys. Rev. Lett. **109**, 245001 (2012)
[9] C.A. Jones, et al., Icarus **216**, 120 (2011)
[10] G.A. Glatzmaier, et al., Geophys. Astrophys. Fluid Dyn., **103**, 31 (2009)